

A novel method based on a force-feedback technique for the hydrodynamic investigation of kinematic effects on robotic fish

Li Wen, Tianmiao Wang, Guan hao Wu and Jinlan Li

Abstract—In this paper, techniques of force-feedback control are applied to the hydrodynamic study of a laboratory robotic fish. The experimental apparatus which allows a robotic model to accelerate from rest to a steady speed under self-propelled conditions is clearly described. In the current apparatus, the robotic fish is mounted on a servo guide rail system and the towing speed is not preset but determined by the measured force acting on the body of the fish. Such an apparatus enables the simultaneous measurement of power consumption, thrust efficiency and speed of a robotic model obtained under self-propelled conditions. The thrust efficiency of the robotic fish can be estimated based on a 2-D vortex ring force estimation method. By comparing the thrust performance of carangiform body-shaped robotic swimmer with different typical BCF (body and caudal fin) swimming modes, i.e. anguilliform, carangiform and thunniform, we show that the robotic swimming fish with the thunniform kinematic movement not only reaches a higher steady swimming speed but is also more efficient than the other two modes. However, in the start phase, using the anguilliform kinematic movement, the robotic swimmer accelerates faster among all kinematic movements. Ultimately, we found that the robotic fish always produce a double-row wake structure no matter which swimming mode used.

I. INTRODUCTION

FISH species such as eels, tuna, and river fish like trout and mackerel include diverse size, shapes and kinematic movements; hence the thrust performance of these fish are very different [1], and the comparative science of fish has long attracted the attention of many scientists. Obviously, the quantitative comparative result of thrust performance is very important for both biologists and engineers, where thrust performance comparison between fish can be made based on thrust efficiency, total power consumption or swimming speed (i.e., Reynolds number). However, the governing kinematic parameters cannot easily be systematically varied with live fish, thus, merely using biological observation methods would lead to an imperfect understanding of the efficient fish swimming mechanisms[2]. In comparison, a robotic experimental apparatus has many advantages: the ability to alter structural parameters such as flexibility,

precise motion control, accurate measurement of locomotors' forces, and the ability to explore a broader parameter space of kinematic movements than exists in live animals. The laboratory hydrodynamic experimental apparatus also allows robotic fish with specific movement patterns and simultaneous measurement of multiple hydrodynamic results.

Many problems still hinder measuring the thrust performance of robotic fish, such as the important metric of biological thrust performance, and the thrust efficiency which is conventionally defined by the following [3,4]: $\eta = UT/P_{fluid}$, where U denotes the self-propelled speed, T denotes the thrust force, and P_{fluid} denotes the pure power consumption in the fluid. The measurement of thrust force cannot be carried out by directly using force transducers, because both thrust and drag forces are produced while the fish is swimming. However, the recent availability of high-resolution, particle image velocimetry [5] has made it possible to measure the wake in the two dimensional plane around the swimming fish. This measurement technique, used by many researchers [6,7,8], had raised the possibility of estimating the pure thrust force T . The P_{fluid} can be obtained from time-averaged fluid power using several approaches [9,10]. Scheultz-suggested estimating the wake power generated by the fish as the fluid power [11]; however, the wake power is only one component of the total fluid power [1,3]. An alternative approach is to subtract the mechanical power (measured in air) from the total power consumed by the motors [9,12,13], from which the fluid power can be obtained.

Therefore simultaneous measurement of power consumption, external force, flow visualization and self-propelled speed of the robotic fish should be investigated by experiments. It should be noted that, in most conventional hydrodynamic experimental approaches of robotic model[14~18] that are shown in Fig.1, the net axial force is not zero, i.e. $T \neq 0$, the excess force is absorbed by the external apparatus, thus the robotic fish was not self-propelled, but moved at a constrained imposed flow, and there was no equality between the thrust and drag. Taking both the active and passive towing methods into consideration, we propose a novel experimental approach based on a force-feedback control technique which combines the advantages of both methods. Using this method, the robotic model would not be subject to external constraints but simply find its own velocity via the force acting upon it. Simultaneous measurement of power consumption, external force, flow visualization and self-propelled speed of the robotic fish can be implemented.

As an engineering and scientific question which was proposed recently by both biologist and engineers [1,23], **what would happen if a carangiform body swims like an anguilliform and/or a thunniform swimmer?** Current experimental method can be used to systematically compare

Manuscript received September,15, 2010. This work was supported in part by National Outstanding Youth Science Foundation support projects, China, under contracts 60525314.

Li Wen, Tianmiao Wang are with the robotic institute in school of Mechanical Engineering and Automation, Beihang University, Beijing 100083, P.R.China, author for correspondence: phone:86-010-82338033; fax:86-010-82338271.

Guanhao Wu is with the State Key Laboratory of Precision Measurement Technology and Instruments, Department of Precision Instruments, Tsinghua University Beijing, China. Jinlan Li is with the department of Electrical and Computer Engineering, National University of Singapore, Singapore (lijinlan@nus.edu.sg)

Author for correspondence: alex.wenli@gmail.com

the swimming performance between different kinematic movements and explore this issue proposed above.

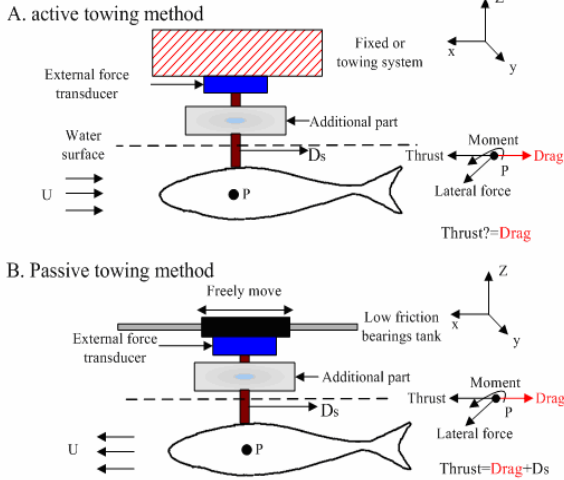


Fig. 1. Schematic view to illustrate the two main conventional categories of flexible fish hydrodynamic test methods. (A) Using the active towing method, the fish model is attached to a strut that holds the robotic model vertically below the towing system or carriage, P denotes the robotic fish center of mass, U denotes the preset flow speed. The total external force acting on the center of mass is shown, expressed as lateral force, thrust, drag and moment. (B) Using the passive towing method, the robotic fish is free to move upstream and downstream on a low friction air bearing system, where the thrust equals the drag force plus the strut force.

II. MATERIALS AND METHODS

A. Description of experimental apparatus

The following section will introduce the method of implementing a self-propelled robotic swimmer on an ordinary servo towing system. Fig.2a shows the mechanical components of a self-propelled experimental apparatus, where the robotic fish model and its affiliated components are fixed under a multi-component force transducer which is attached to the carriage by screws. The robotic fish is submerged under water, while its transmission mechanism is mounted on a metal plate and is above the surface of the water. The external force of a robotic fish is measured using a multi-component piezoelectric force transducer (Kistler 9254C) which is assembled vertically above the robotic fish model, and has a natural frequency of 3 kHz, a high rigidity of 500 N/um, and a sensitivity of 0.005 N in the axial direction. The control unit and power supply of the robotic fish, and the laser system and camera used for flow visualization, are all mounted on a carriage rest which is belt-driven on rails which run along the towing direction (the x direction). The water tank, which is 7.8 m×1.2 m×1.1 m, is filled with water, and provides the robotic model with sufficient space to move without being affected by the boundaries on both sides. The fish model is also located at mid-depth in the tank to avoid any interference effects from the free surface and the bottom of the tank. The output of the external Kistler transducer is recorded by computer I (as shown in Fig.2) through a connecting cable using a CAN bus (Controller Area Network bus).

A particle image velocimetry (PIV) system which is also fixed on the carriage is used to measure the flow patterns

generated by the robotic fish. The laser beam (4W) of wavelength 0.532 μm is expanded by two cylindrical lenses to generate a light sheet which is reflected successively by three mirrors into the water tank passes through the middle line of fish (see Fig. 1). The flow is visualized by seeding the water with nylon particles (40-70 μm , 1.05 g cm^{-3}) to reflect the laser light. A high speed CCD camera (100fps, 1024 pixels × 1024 pixels) is used to record the particle images in the wake.

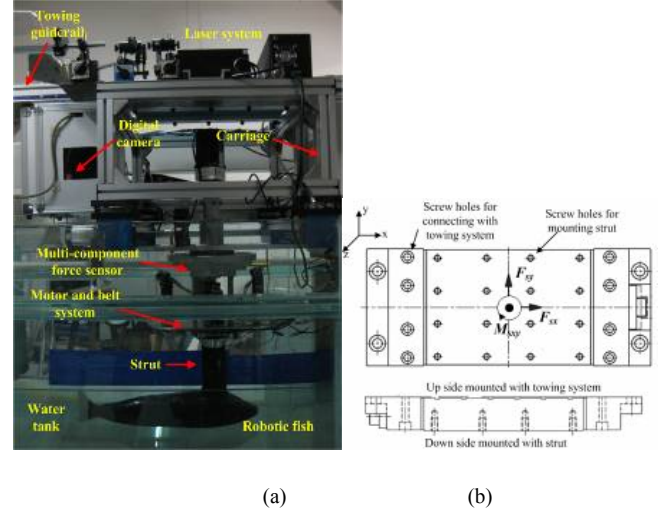


Fig.2 (a) Snapshot of the self-propelled experimental apparatus with the laser shut down. (b) Illustration of forces acting on the multi-component force transducer. F_{sx} , F_{sy} , M_{xy} are the instantaneous external forces measured by the multi-component force transducer in the x (forward) direction, the y (lateral) direction and the rotational moment at the center of the transducer, respectively.

B. Method for self-propelled fish

Fish swim in water by propelling themselves with active deformation of their body and tail. The mechanism of the self-propelled fish's undulating body in a medium is determined by the interaction of the fish's body movement and the varying fluid dynamics. In this study we only consider fish swimming in a forward direction with lateral and rotational direction constraints. The non-inertial reference frame is attached to the fish's center of mass. It should be noted that this simplified method (e.g. constrained lateral and rotational direction in a 2D plane) is widely employed in both experimental and numerical investigations of straight-line hydrodynamic thrust performance [4,24]. From Newton's law of momentum, equations for the fish in the forward axial direction will satisfy:

$$F_x = m_f \frac{dU}{dt}, \quad (1)$$

where F_x denotes the net axial force in the forward direction, U represents the fish's self-propelled speed in the forward direction, and m_f represents the mass of the robotic fish. As shown in Fig.2b, the force about the center of the multi-component force transducer (expressed by P as shown in Fig.2b) will satisfy the following:

$$F_x + F_{sx} + D_s = (m_f + m_a) \frac{dU^T}{dt}, \quad (2)$$

where m_a denotes the mass of the additional parts under the force sensor excluding the robotic fish. The mass of the additional parts in the current experimental apparatus (also in most previous test instruments used) includes the following: the inherent mass of the multi-component force transducer, the mass of the robotic fish's actuators, the mechanical transmission system and the streamlined strut which penetrates the water to connect with the robotic fish's head. U^T represents the forward speed of point P . Because the force transducer is fixed firmly to the towing carriage, U^T denotes the forward speed of the towing system.

Equation 1 represents the self-propelled condition of the robotic fish in the forward direction. Suppose the speed of the towing system U^T equals speed U of the self-propelled fish in Equation 1 ($U=U^T$), combining Equation 1 with 2 now gives:

$$\frac{dU^T}{dt} = \left(\frac{F_{sx} + D_s}{m_a} \right). \quad (3)$$

Thus, the right hand side of Equation 2 can be replaced by Equation 4, then Equation 5 can be obtained:

$$F_x + F_{sx} + D_s = (m_f + m_a) \left(\frac{F_{sx} + D_s}{m_a} \right) \quad (4)$$

$$F_x = m_f \left(\frac{F_{sx} + D_s}{m_a} \right) = m_f \frac{dU^T}{dt}. \quad (5)$$

While the robotic fish has a certain kinetic movement, with Equations 1 and 5, it is obvious that $dU^T/dt = dU/dt$. As the self-propelled speed $U(t)$ simply satisfies the conditions of continuity and differentiability, and the initial boundary condition satisfies $U(0) = U^T(0) = 0$ and $dU^T/dt = dU/dt = 0$, then $U(t) = U^T(t)$ can be obtained. Equation 3 can be considered as the necessary and sufficient condition of $U(t) = U^T(t)$.

From the above deductions, the following coupled dynamic processes appear: 1) The fish body deforms following certain kinematic movements; 2) The net axial forward force body is measured by the multi-component force transducer; 3) The forward traveling speed of the towing system which is rigidly linked with the fish's center of mass will be decided by axial force feedback. This means that when a robotic model performs a certain undulating movement, it can satisfy a self-propelled condition in the forward direction. The robotic model will not be influenced by the constraining effect of the towing system, just as if it was freely swimming in the water. To relate the measured force to the controlled speed of the towing system, we represent Equation 3 by the time-discrete form:

$$[U^T(t) - U^T(t - \Delta t)] / \Delta t = \frac{F_{sx} + D_s}{m_a}. \quad (6)$$

Equation 6 governs the forward speed U^T with the force feedback. Even a small change in F_{sx} will be fed back, corresponding to a change in U^T by the towing system. The measured forward force at time t can be denoted as $F_{sx}(t)$, and this force can now be used to compute the forward velocity. However, rather than using the newly measured force in Equation 6, a weighted average force is used instead as given by the following:

$$\bar{F}_{sx}(t) = \sigma F_{sx}(t) + (1 - \sigma) F_{sx}(t - \Delta t) \quad (7)$$

where σ is the weighting factor commonly chosen to be between 0.5 and 1.0. The actual experimental result showed that the optimal choice for σ is 0.85, while below this value the whole towing system becomes unstable and waking occurs, whereas increasing σ from 0.85 to 1 reduces the accuracy of the force feedback speed. Using the weighted force as given above, Equation 6 can be rearranged as in the following equation to give:

$$U^T(t) = \left(\frac{\bar{F}_{sx} + D_s}{m_a} \right) \Delta t + U^T(t - \Delta t) \quad (8)$$

The forward force F_{sx} will be transmitted to the motion coordinator (Trio MC206) for speed control (denoted by $U^T(t)$) based on Equation 8. **As described above, the laboratory robotic fish model fixed on a towing system can work under a self-propelled condition**, and the lateral force and the external rotating moment can be measured simultaneously during the experimental runs.

C. Robotic fish design and power test

This section provides a brief introduction to robotic carangiform swimmer design and power measurement. The robotic fish model had a total length of 0.588m and consisted of a streamlined main body capable of flexing, with a rigid propulsive tail fin (See Fig.3A). The outer shape of the robotic fish was an exact replica of the shape of a typical carangiform swimmer, the mackerel (*Scomber scombrus*) whose body shape parameters have been adequately provided[24]. Considerable effort was also made to imitate the internal mass distribution of a live swimming fish in the robotic fish's body. The mechanism was a high-precision assembly of 4 links made from anodized aluminum and covered with foam and a special waterproof structure made of silica. Fig.3A provides details of the fabrication of the robotic fish. Each mechanical link was capable of relative rotation with respect to its neighboring link and was driven by a brush servo motor, mounted on a metal plate above water. All the links were independently controlled by a motion coordinator, the Trio MC206, and belts transmitted the motion to individual links with minimal frictional forces using bearings which were assembled on the shafts, as shown in Fig.3B. Because a waterproof outer skin was used to envelop the whole multilink mechanical skeleton, it was capable of fishlike undulation with the form of an actual swim fitting curve. The pair of activating belts per motor that drive the mechanical parts were linked to move laterally and emulate a fish swimming. All the belt movements were transmitted by four transmission shafts which are shown in Fig.3D and ran through the streamlined low-drag vertical strut (as shown in Fig.3C). Finally these shafts entered the fish body and drove the individual links.

The fluid power is given by Equation 9, where P_f is the pure fluid power, P_T and P_M are the total measured motor power and mechanical power when driving the robotic fish in water and in air. The instantaneous power into the motor is found as $P_j = M_j \omega_j$, where the ω_j denotes the angular speed of the motor. The angular speed is obtained through the differential value of a potentiometer which built in the fish's body as can be seen in fig.3B, and $\omega_j = d(\theta_j)/dt$. In addition, the torque

constant K_M links the mechanical torque M_i with the electric current I_i by using the equation $M_i = K_M I_i$, where $K_M = 0.03 \text{ Nm/A}$ for the motor used.

$$P_f = P_T - P_M \quad (9)$$

We measure the circuit measurements of the discrete links across the analog input channels on the data acquisition card P325, where the sampling rate is set as 200Hz. The total average power consumption of the fish body within a period is given by Equation 10.

$$P = \frac{\int_0^T \sum_{i=1}^{i=4} M_i(t) \omega_i(t) dt}{T} \quad (10)$$

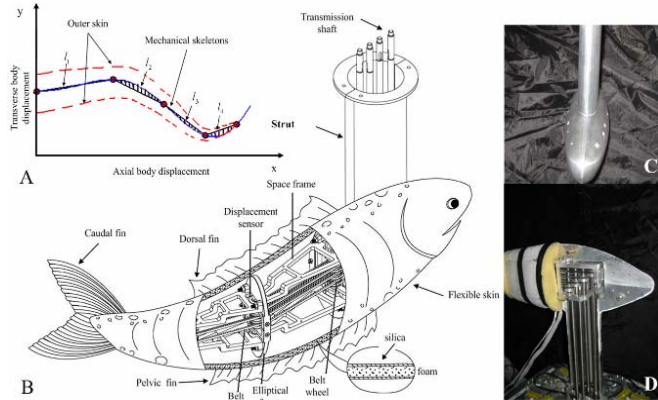


Fig.3. (A) Actuation mechanisms of the relative rotations of the robotic links and the actual fitting curve, versus the reference body wave in the robotic fish, where $x=0$ is located at a distance 30 % along the body length. (B) Schematic view of the robotic Saithe and its inside implementation. (C) Low drag streamlined vertical strut which is connected with fish's head. (D) Four transmission shafts which ran through the streamlined low-drag vertical strut.

D. Flow visualization and Thrust estimation

We used an 'mpiv' toolbox, which had been tested, was shown to be robust and had sufficient accuracy to obtain the flow velocity vectors and vorticity. The vortex ring model which assumes that all the energy shed by the robotic fish is contained in circular vortex rings was used for the analysis of the wake. The cross-sectional view through a vortex ring consisted of two vortices in opposite rotation. The morphology of a vortex was described for the vortex center as having a core radius R_0 , ring radius R , momentum angle ϕ and jet angle α . The definitions and estimates of these parameters were as previously described in live fish observations [7,25,26].

The impulse I of a vortex ring can be calculated as:

$$I = \rho \Gamma A, \quad (11)$$

where ρ is the density of water, A is the area surrounded by the vortex ring, and Γ is the mean absolute value of the circulations of the pair of vortices. Circulation Γ is the line integral of the tangential velocity component \overline{V}_T about a curve C enclosing the vortex:

$$\Gamma = \oint \overline{V}_T d\vec{l} \quad (12)$$

Where $d\vec{l}$ is the differential element along the curve C . The time-averaged thrust force F can be calculated as:

$$F = I / T, \quad (13)$$

where T is the time over which force is generated.

III. RESULTS

A. Kinematic movements and hydrodynamic definitions

The kinematic movements for all typical BCF swimmers which gently start from rest to a steady swimming mode, as approximately fitted from the observed results of a live swimmer [21], can be expressed by the following:

$$h(x,t) = a(x)a(t)\sin(kx - \omega t) \quad (14)$$

The $h(x,t)$ denotes the fish kinematic movement function in a body-fixed coordinate system with x measured starting from the nose of the robotic fish, and k denotes the wave number, where $k=2\pi/\lambda$. λ denotes the wavelength, while ω denotes the circular frequency of oscillation. c_1, c_2 can be adjusted to achieve a specific value for the amplitude envelope for entire body, and L represents the fish body length. As Equation 15 shows, the robotic fish undulates the posterior part (i.e. $x > 0.33L$) of the body from rest ($t=0$) to steady periodic undulation ($t > t_0 = 1.0T$) after a gentle transition process ($0 < t < t_0$). As mentioned previously, our robotic model shape followed the replica of a mackerel with a fusiform body and relatively separate tail. The carangiform is intermediate between the anguilliform and thunniform swimmer, unlike the anguilliform fish, whose body is a fairly constant oval cross-section and has no physical demarcation between the "tail" and "body", or the thunniform fish, which has a distinct narrower peduncle and large aspect ratio caudal fin, as can be seen in Fig.5.

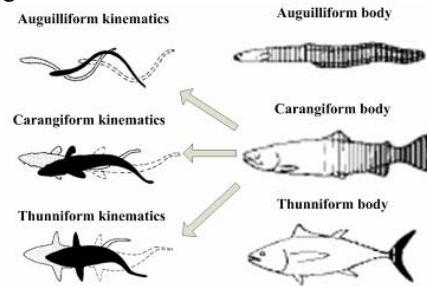


Fig.5 Different BCF swimming pattern, inspired by Sfakiotakis

For anguilliform kinematic movement, the non-dimensional wavelength is set as $\lambda/L=0.65$ [3], $\lambda/L=0.95$ for a carangiform swimmer [21], and $\lambda/L=1.25$ for a thunniform swimmer [27]. In this paper, for all kinematic movements, the tail beat amplitude h was set to $0.1L$, and the following values were used for the coefficients $c_1=0.03$ and $c_2=0.04$ to match the displacement at the caudal fin tail end where $h=0.1L$. Fig.5 also shows the body deforming shape for three distinct kinematic movements. The purpose of the present study initially is to investigate and quantify the hydrodynamic effects of the swimming kinematic movements. We will conduct robotic self-propelled swimmers of a fixed body shape (mackerel) with different kinematic movements; therefore, we can compare the performance of a mackerel body swimming like an eel (anguilliform kinematic movement) with that of a tuna (thunniform kinematic movement) and a mackerel (carangiform kinematic movement) itself.

The mean quantities of force, thrust, power and efficiency are obtained by averaging the instantaneous values over several swimming cycles at a steady swimming state. Several important non-dimensional kinematic movements and

hydrodynamic parameters are introduced: (1) the Reynolds number Re at a steady swimming state, which is defined as UL/ν , where U represents the mean steady swimming speed, L represents the fish length, ν is the kinematic movements viscosity of the water; (2) The St (Strouhal number) which is defined as $2fh/U$. Furthermore, the thrust efficiency is already defined in the introduction. It is also important to note that the thrust efficiency should only be obtained under constant-speed swimming conditions when the robotic fish has reached its quasi-steady state of constant-mean velocity.

B. Kinematic movements and hydrodynamic results

1. Kinematic movements and force results

First we obtained the speed results of a self-propelled robotic fish, under the same environmental conditions (i.e. water temperature and immersed depth of fish body). Three different kinematic movements were performed with the same tail-beat frequency ($f=0.8\text{Hz}$) and undulating amplitude ($h=0.1L$). The force feedback control was continued for 20s, a time duration which is long enough for the swimmer starting from rest to reach the quasi-steady steady swimming state. The self-propelled swimming speed time history for the three kinematic movements are all displayed in Fig.6a.

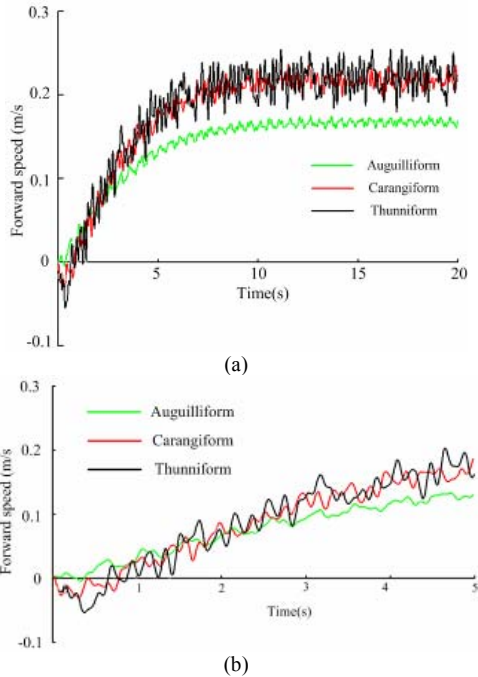


Fig.6 Self-propelled swimming speed and force time history for the three kinematic movements. (a) Speed history of three kinematic movements. (b) Speed fluctuation of hybrid kinematic movements.

During the initial 12 flapping circles, which totally take about 10s, all three kinematic movements reached the steady swimming mode in succession. Different constant-mean speeds were observed, and robotic fish with carangiform and thunniform kinematic movements reached higher velocity, with thunniform having a slight predominance over carangiform. Considering the average speed in a steady state, the thunniform kinematic movement was 29.7% faster than the anguilliform, and 2% faster than the carangiform, as reported in Table 1. We used the St number as a measure of ‘hydrodynamic thrust performance’, as defined previously. The lower the value the of the St number, the faster the robotic

fish swam for a given input flapping frequency and amplitude. The St number results were 0.55, 0.43, 0.424 for anguilliform, carangiform and thunniform. A very interesting finding can be observed in Fig.6b, which is that during the initial acceleration phase, the swimmer with the anguilliform kinematic movement accelerated faster than the other two types of movement. Moreover, the other two types of kinematic movements initially had negative speed, while the anguilliform had positive speed throughout. Ultimately, the swimmers with carangiform and thunniform overtook the anguilliform kinematic movement and finally performed better. This trend has also been documented in a number of experiments on live swimmers [30,31], which suggests that fish might change their inherent kinematic movement during the start to achieve better performance.

2. Hydrodynamic results

Considering the total power consumption, as can be seen from Table 1, the non-dimensional power of the carangiform kinematic movement has higher value than the other two types, and again, the thunniform kinematic movement has the minimum power coefficient. Tytell [1] reported that a trout (carangiform swimmer) has a larger estimated wake power than an eel (anguilliform swimmer), which is in agreement with present experimental results. One interesting observation was that with the same body, the thunniform kinematic movement has the least power coefficient compared with other types of BCF movements.

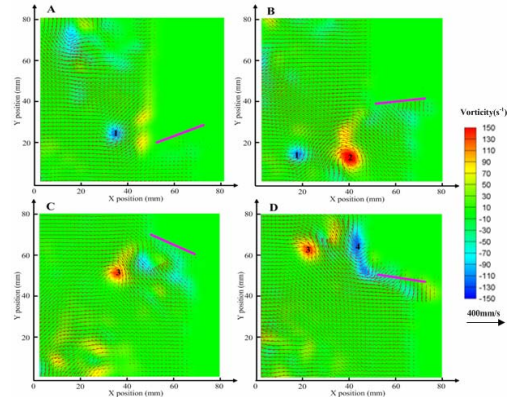


Fig.7 Wake generated by the robotic swimmer using the thunniform kinematic movement, where the pink drawn line indicate the position of robotic fish’s caudal fin, A~D show the evolvement of vorticity and flow vector field at four different times of a flapping period: $T/4$, $T/2$, $3T/4$, T , respectively. Note that the vortex number is placed approximately in the center of the vortex.

Considering the wake structure of robotic fish, in the horizontal PIV plane, each 3D ring appears as a pair of 2D vortices, and for the current robotic fish using all three kinematic movements, i.e., anguilliform, carangiform and thunniform, creates two vortex pairs in the near wake for each flapping circle. Fig.7 shows the PIV time-series of vorticity fields for the thunniform kinematic movement. In each flapping cycle, the tail performed two flicks, a flick to its right side and then a flick to its left side. Each flick of the tail generated a pair of vortices (Fig.7B, vortices 1 and 2 from the left (up in the figure) flick, Fig.7D, vortices 3 and 4 from the right (down in the figure) flick). After the vortices are shed, they are characterized by lateral divergence and spreading away from the body axis in a wedge-like arrangement.

Considering the large-scale characteristics of the wake structure, this type of wedge-like double-row wake has been observed in the study of an oscillating flat plate [13], and the CFD studies by Borazjani [28] for a carangiform swimmer at a relatively high St number ($St=0.6$).

While the wake structure of live carangiform swimmers always showed a single-row vortices such that a jet flow is formed between the vortices, which have been called a reverse Karman street [6,7,33], the double row wake patterns have never been observed and reported experimentally for a carangiform swimmer. This experiment provided a robotic fish with the same body shape and kinematic movement (the carangiform kinematic movement) as that of a live carangiform swimmer. However, a question remains about the disparity between the wake structures shed by a live fish, and a robotic swimmer. Recent computational results and experimental studies with flapping foil indicated that the wake structure was dependent primarily on the St number. The dependence of the wake structure on the St can be viewed as the ratio of the average caudal fin heave velocity to the axial forward swimming speed. Noting that carangiform swimmers in nature undulate their bodies at an St in the range of 0.25~0.35 [34], we observe in the current experiment results an St number ranging between 0.424~0.55, which indicates the self-propelled steady swimming speed of robotic fish is lower than that of live fish. As a self-propelled robotic fish travels at a higher St number, the shedding vortices from the caudal fin tend to have a larger velocity component, which advects them away from the midline of the body and causes them to spread in the lateral direction, therefore, the wake splits laterally and the double row pattern emerges.

Considering the thrust efficiency of robotic fish, to the best of our knowledge, there is no previous report on experimental quantitative values of thrust efficiency on robotic fish, which could be because it is complicated to implement the required experimental apparatus. Currently, the final experimental thrust efficiency for robotic fish is 47.3 % for the thunniform kinematic movement, 31.4 % for the carangiform kinematic movement, and 26.6 % for the anguilliform kinematic movement. The thunniform kinematic movement not only reached higher velocities but also obtained the best thrust efficiency of all the types of kinematic movements. Compared with results from previous numerical studies, the efficiency values we obtained in this work using experimental approaches seem quite reasonable. For example, a value of 47.5% was reported from the results of the 3-D computational result of a swimming mackerel under inviscid conditions by Borazjani [28].

Table 1: Variables for hydrodynamic quantities and comparisons, where the three cases represent a swimming race result for three BCF swimming kinematic movements

Variable	Abbreviation	Anguilliform	Carangiform	Thunniform
Speed(m/s)	U	0.171	0.218	0.221
Strouhal number	St	0.55	0.43	0.424
Ratio of wave speed	δ	1.78	2.04	2.66
Power coefficient	C_p	0.0032	0.0033	0.0031
Thrust efficiency	η	26.6%	31.4%	47.3%

IV. CONCLUSION AND DISCUSSION

The present method differs from previous experimental methods in that the forward swimming speed and acceleration of the robotic fish has not been imposed but has been created from the force acting on the robotic swimmer. The generalizability of the experimental method and apparatus discussed here indicates that many broader issues can be investigated using the present method, to simultaneously understand how external hydrodynamic force is generated, power is consumed, and wake structure is formed under self-propelled conditions. However, our present work cannot conclusively determine whether the differences we found in thrust performance (i.e. thrust efficiency, power, swimming speed) are due to body undulation or caudal fin movement. It is reasonable to postulate that both body undulation and caudal fin movement should play a role but to what extent each factor contributes is not known. In our future work, more systematic investigation of the parametric dependence of principal parameters on the efficient swimming of robotic fish will be carried out.

REFERENCES

- [1] Tytell, E. D., *Exp. Fluids*, **43**, 701-712. (2007)
- [2] Lauder, G. V., Anderson, E. J., Tangorra, J. and Madden, P. G. A., *J. Exp. Biol.* **210**, 2767-2780 (2007).
- [3] Tytell, E. D., *J. Exp. Biol.* **207**, 3265-3279. (2004)
- [4] Lighthill, M. J., *Ann. Rev. Fluid Mech.* **1**, 413-446. (1969)
- [5] Willert C *Meas Sci Technol.* **8**,1465-1479, (1997)
- [6] Muller, U. K., Van Den Heuvel, B. L. E., Stamhuis, E. J. and Videler, J. J., *J. Exp. Biol.* **200**, 2893-2906. (1997)
- [7] Nauen, J. C. and Lauder, G. V., *J. Exp. Biol.* **205**, 1709-1724. (2002)
- [8] Drucker, E. G. and Lauder, G. V., *Integr. Comp. Biol.* **42**, 243-257. (2002)
- [9] Buchholz, J. H. J. and Smits, A. J., *J. Fluid Mech.* **603**, 331-365. (2008)
- [10] Anderson, J. M., Streitlien, K. and Barrett, D. S. *J. Fluid Mech.* **360**, 41-72. (1998)
- [11] Schultz, W. W. and Webb, P. W. *Integr. Comp. Biol.* **42**, 1018-1025. (2002)
- [12] Barrett, D. S., Triantafyllou, M. S. and Yue, D. K. P. *J. Fluid Mech.* **392**, 183-212. (1999)
- [13] Buchholz, J. H. and Smits, A. J. *J. Fluid Mech.* **546**, 433-443. (2006)
- [14] Bandyopadhyay, P. R., *IEEE J. Ocean Eng.*, **30**, 109-139,(2005).
- [15] Beal, D. N., Hover, F. S., Triantafyllou, M. S., Liao, J. and Lauder, G. V., *J. Fluid Mech.* **385**-402 (2006).
- [16] Guang-Kun Tan, Gong-Xin Shen, Shuo-Qiao Huang, *Experiments in Fluids*, **43**, 811-821 (2007).
- [17] Brucker C, Bleckmann H, *Exp Fluids* **43**:799–810, (2007)
- [18] Tangorra J, Anquetil P, Fofonoff T, Chen A, Del Zio M, Hunter, *Bioinsp Biomimet* **2**:S6–S17, (2007)
- [19] G. V. Lauder, E. J. Anderson, J. Tangorra, Peter G. A. Madden, *J. Exp. Biol.*, **210**, 2767–2780 (2007).
- [20] K. Morgansen, V. Duindam, R. Mason, J. Burdick, and R. Murray, *IEEE Int. Conf. Robot. Autom.* 427–434, (2001).
- [21] Videler J J. *Fish Swimming*[M].London: Chapman & Hall. (1993).
- [22] Borazjani, I. and Sotiropoulos, F., *Phys. Fluids* **21**, 091109. doi:10.1063/1.3205869. (2009)
- [23] Iman Borazjani, Fotis Sotiropoulos, *J. Exp. Biol.*, **212**, 576-592 (2009).
- [24] Hess, F. and Videler, J. J. *J. Exp. Biol.* **109**,229–251,(1984).
- [25] Wu G H, Yang Y, Zeng L J. *Review of Scientific Instruments*, **77**, 1143-02. (2006).
- [26] Wu G H, Yang Y, Zeng L J. *J. Exp. Biol.*, **210**, 2181-2191.(2007).
- [27] HEIDI DEWAR AND JEFFREY B. GRAHAM, *J. exp. Biol.* **192**, 45–59 (1994)
- [28] Borazjani, I. and Sotiropoulos, F. *J. Exp. Biol.* **211**, 1541-1558. (2008)
- [29] Iman Borazjani, Fotis Sotiropoulos, *J. Exp. Biol.*, **212**, 576-592 (2009).
- [30] Weihs, D.. *J. Theor. Biol.* **48**, 215-229. (1974)
- [31] Domenici, P. and Blake, R. W., *J. Exp. Biol.* **200**, 1165-1178. (1997)